ADVANCED FUNCTIONAL MATERIALS
www.afm-journal.de

Understanding and Controlling the Self-Folding Behavior of Poly (*N*-Isopropylacrylamide) Microgel-Based Devices

*Xue Li and Michael J. Serpe**

Poly(*N*-isopropylacrylamide) (pNIPAm) microgel-based materials can be fabricated that self-fold into three-dimensional structures in response to changes in the environmental humidity. The materials are composed of a semi-rigid polymer substrate coated with a thin layer of Au; the Au layer is subsequently coated with a pNIPAm-based microgel layer and finally covered with a solution of polydiallyldimethylammonium chloride (pDADMAC). The pDADMAC layer contracts upon drying causing the material to deform (typically bending); this deformation is completely reversible over many cycles as the environmental humidity is systematically varied. Here, by varying the size and aspect ratio of the polymer substrate, it is possible to develop a set of empirical rules that can be applied to predict the material's self-folding behavior. From these rules, materials that self-fold from two-dimensional, flat objects into discrete three-dimensional structures, which are fully capable of unfolding and folding multiple times in response to humidity, are designed.

1. Introduction

Materials that spontaneously undergo a change in structure, for example, from a two dimensional (2D) to three dimensional (3D) structure in response to external stimuli have been of great interest as artificial muscles, and for fabricating novel actuators, switches, valves and in robotics.[1–6] Various stimuli responsive polymers have been identified, which exhibit responses to electric fields, temperature, light, pH, ionic strength, humidity, and/or solvent composition.[7–11] Recently, responsive hydrogels and polymer-based films have been used as materials capable of converting chemical or physical energy into mechanical forces, which can lead to macroscopic changes to a material's conformation.[12] Specifically, temperature responsive poly(*N*-isopropylacrylamide) (pNIPAm) based hydrogel sheets capable of transforming from a planar state to a 3D structure have been developed by tuning the concentration of monomers and crosslinking density in the hydrogel sheets.[13] Regions with different polymer content went through differential deformation upon heating allowing the formation of unique 3D structures. Wang et al. recently fabricated near-infrared light-driven hydrogel actuators by interfacing reduced-graphene oxide sheets with protein-based polymers. These hydrogels showed rapid, reversible bending motion at specific positions where near-infrared laser was applied.[14] Another system composed of a soft poly (butadiene) phase and a hard metal – ligand phase was developed, which exhibited shape-memory properties in response to external stimuli.[15] In this case, the key component in fulfilling the shape change is the metal–ligand phase which can become soft when exposed to a variety of stimuli (e.g., light, heat, chemicals).

Of recent, several types of humidity responsive polymers have also been used to fabricate actuators. For example, Langer and co-workers[16] recently developed a polymer composite of rigid polypyrrole (PPy) embedded with a flexible polyol-borate network. PPy can absorb water and change its shape, while the soft polyol-borate network is also sensitive to water, undergoing hydrolysis and reformation of the borate ester crosslinker upon water absorption and desorption, respectively. By breaking and reforming intermolecular hydrogen bonding between PPy and the polyol-borate network and the borate ester within the polyol-borate network upon water sorption and desorption, the film shows expansion and contraction, resulting in the film's rapid and continuous locomotion. In another example, Sun and co-workers developed one bilayer film consisting of a polyeletrolyte multilayer (PEM) film and a layer of UV-cured prepolymer.[17] The PEM is a film of thermally crosslinked poly (acrylic acid) (PAA)/poly(allylamine hydrochloride) (PAH). The PAA/PAH is able to absorb/desorb water with increasing/decreasing environmental humidity, which resulted in swelling/shrinking of the layer. They fabricated an energetic walking device driven by the powerful humidity responsive PEM.

In this contribution, we show that poly(*N*-isopropylacrylamide) (pNIPAm) microgel-based materials are capable of reversible self-folding into unique 3D structures in an atmosphere of varying humidity. PNIPAm is one of the most well-known and well-studied thermoresponsive polymers. PNIPAm-based macroscopic and colloidal hydrogels (nanogels or microgels, depending on their diameter) are easily synthesized, and have found numerous applications.[18–21] Furthermore, these materials can be synthesized to respond to additional stimuli other than temperature via copolymerization of various functional monomers (co-monomers) at the time of their synthesis.[22,23] One of the most commonly studied co-monomers is acrylic acid (AAc), which has a pKa of approximately 4.25.

X. Li, Prof. M. J. Serpe
Department of Chemistry
University of Alberta
Edmonton, AB T6G 2G2, Canada
E-mail: michael.serpe@ualberta.ca

DOI: 10.1002/adfm.201400201

PNIPAm-co-AAc microgels swell when the solution pH > 4.25 due to the deprotonation of AAc increasing the charge-charge repulsion inside the network of microgels. As such, at high pH, the microgels can be considered as polyanions.

Recently, layer-by-layer assembled films of alternating polyanions and polycations have emerged as an important soft materials which showed repeated deformation in response to different stimuli.[22,24] Polydiallyldimethylammonium chloride (pDADMAC) is a homopolymer of diallyldimethylammonium chloride (DADMAC) and a high charge density cationic polymer (polycation), which has been applied to fabricate various advanced materials by layer-by-layer self-assembly.[25] In the dry state, PDADMAC is also responsive to humidity, exchanging water with the environment and inducing contraction and expansion of the polymer.[5] In this submission we show that by exploiting the individual characteristics of the pNIPAm-co-AAc microgels and the pDADMAC, and their electrostatic interactions, a polymer-based material capable of reversible deformations is achieved. Furthermore, by investigating the self-folding behavior of devices with different dimensions, a mathematical model to predict the behavior was developed. Finally, by using this mathematical model, we could predict the self-folding behavior of the devices, which could then be used to design materials that self-fold into desired three-dimensional structures.

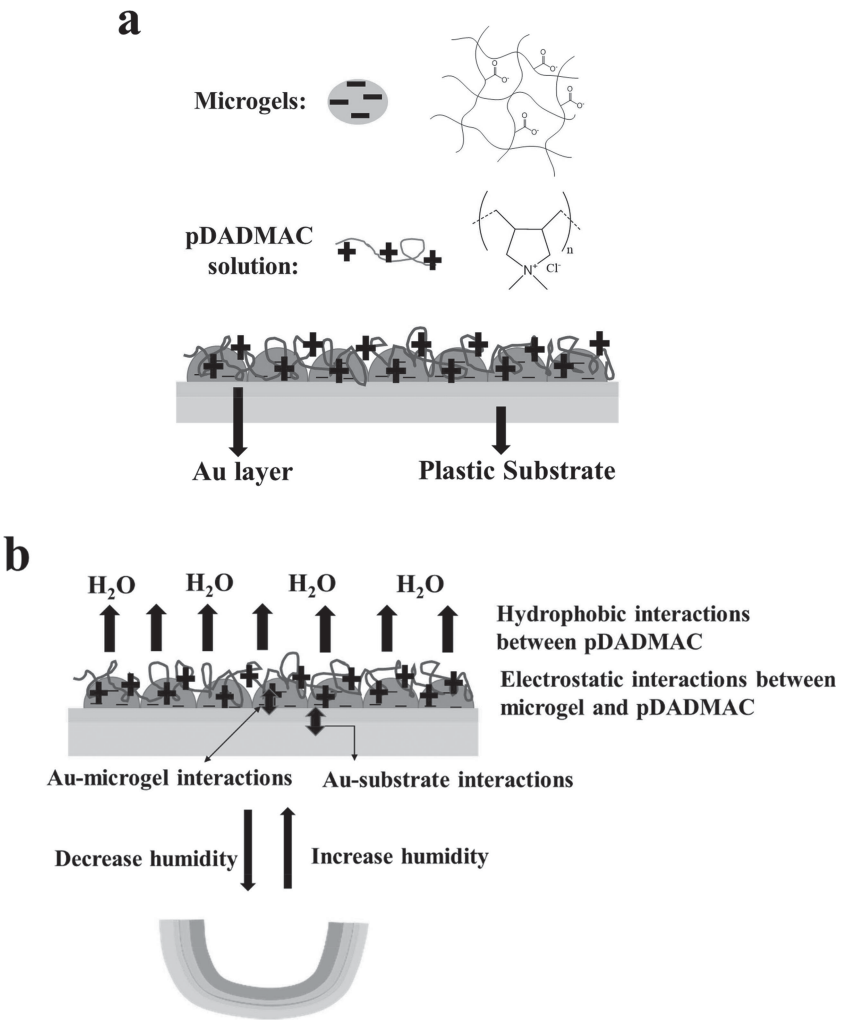

Figure 1. Device construction and self-folding mechanism. a) Devices were constructed by depositing a single layer of pNIPAm-co-AAc microgels on a flexible plastic substrate (bottom layer) coated with a Au/Cr layer. A pH 6.5 solution of pDADMAC was subsequently added onto the microgel layer and dried. At this pH, there are strong electrostatic interactions between the negatively charged microgels and the positively charged pDADMAC. b) When the pDADMAC layer dries it contracts, and since there are strong electrostatic interactions between the microgels and pDADMAC layers, and the microgels are strongly bound to the Au–plastic layer, the whole device bends as the pDADMAC layer contracts. If the environmental humidity is increased, the pDADMAC layer resolvates, and the device unbends. This bending/unbending mechanism is completely reversible over many cycles.

2. Results and Discussions

2.1. Mechanism

Previously, we designed pNIPAm microgel–pDADMAC-based devices capable of lifting many times their own mass in response to environmental humidity changes.[5] The devices are fabricated by depositing a monolayer of pNIPAm-co-AAc microgels on a Au-coated plastic substrate (**Figure 1**a). The apparent solution diameter of the microgels used here was 1548 ± 69 nm (measured using differential interference contrast microscopy). The microgels form a homogenous layer, with a thickness that is ≈0.5 of the solution diameter.[21] Subsequently, a specific amount of an aqueous solution of pDADMAC (pH 6.5) was added onto the microgel layer. At this pH, the microgels are negatively charged, while pDADMAC is positively charged. Due to electrostatics, the pDADMAC strongly binds to the microgels, which are strongly bound to the Au substrate. After deposition of the pDADMAC layer, the devices were introduced to a humidity-controlled chamber and allowed to dry at low humidity. Upon drying, the pDADMAC layer contracts due to water evaporation leading to enhanced pDADMAC hydrophobic interactions. As a result of the strong electrostatic interactions between microgels and pDADMAC, together with the strong interactions between gold and microgels, the contraction of the pDADMAC layer causes the device as a whole to deform/bend (Figure 1b). We point out here that the thickness of microgel–pDADMAC composite is on the scale of mm (measured using calipers).

To explain how the device bends/deforms, the device can be thought of as two separate layers (**Figure 2**a). The pDADMAC–microgel composite (upper layer) serves as the device's active layer, while the Au–plastic substrate (lower layer) is the passive layer. Two assumptions were made in this investigation: 1) the pDADMAC–microgel composite is homogeneous and

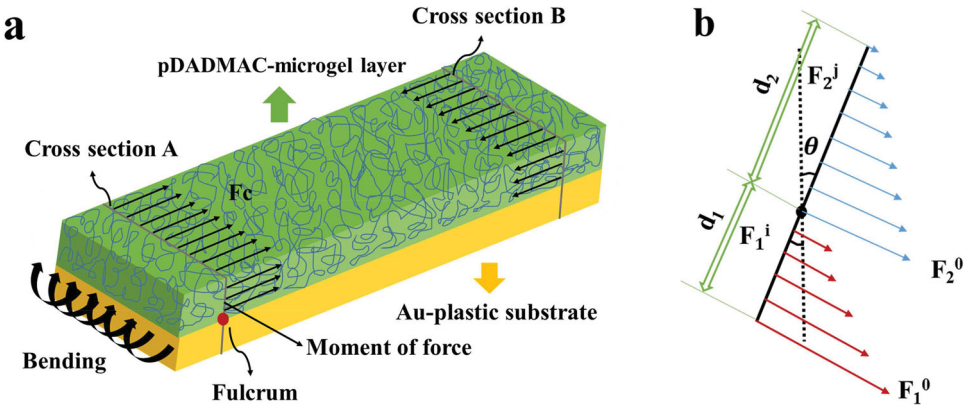

Figure 2. Mechanical model used to describe the devices. a) A detailed view of the device showing the stress generated in the upper layer (F_c), which leads to device bending. The device is considered to be two separate layers, the top layer defined by the pDADMAC-microgel layer and the bottom layer defined by the Au/Cr-coated plastic substrate. b) A single portion of the device in a). The dashed line represents the initial state of the two layers, while the solid line represents the final state after bending is complete. F_1^i are the stresses at different points on the Au–plastic substrate, while F_2^j are the stresses at different points on the microgel-pDADMAC layer. d_1 is the thickness of Au–plastic substrate, while d_2 is the thickness of the microgel-pDADMAC layer. θ is microscopic bending angle. The blue vectors (force vectors in upper layer) represent the contraction forces in the microgel-pDADMAC layer, while the red vectors (force vectors in lower layer) represent the restoring forces in the Au-substrate layer after the bending is complete.

stress along the layer either linearly increases or decreases; 2) the Au–plastic substrate is not contractible and stress along the layer either linearly increases or decreases. The interface between the two layers can be thought of as being made of an infinite number of points, which do not change location because of assumption (2). Each point is defined as a fulcrum, one of which is shown in Figure 2a; the two layers are connected at that/those small region(s). In the active layer, we have shown that dehydration leads to contraction, presumably due to enhanced hydrophobic interactions between the pDADMAC.[5] This contraction leads to contracting forces (F_c), which are shown as black vectors in Figure 2a. The strong forces pull all parts of the Au–plastic lower layer in the direction of force. Meanwhile the lower layer connected to the upper layer by the fulcrum will be pulled in the opposite direction by the torque (τ) generated from the contraction of the upper layer.

To further explain the bending/folding process and to identify the governing parameters, we developed a mathematical model. To make the model less complex, we concentrated on only a "microscopic" portion of the assembly. As shown in Figure 2b, the two layers are represented by two lines connected by one fulcrum. The dashed line represents the initial state of the portion of the assembly considered, while the solid line represents the final state after bending is complete. After bending is complete, the force at the fulcrum (at the interface between the pDADMAC and the microgel–Au–plastic layers) is a maximum, which gradually decreases as the distance from this point increases through the upper layer. The forces are noted as F_2^j indicated by the blue vectors in Figure 2b. This is the case because we assume that the plastic layer is not contractible (assumption 2), therefore we assume that the interface is likewise not contractible. Therefore, the polymer at the interface has more of a restoring force than the fully contracted polymer layer far away from the interface—much like a spring. F_2^j in the upper layer depends on three factors: the microscopic bending angle θ, a material related force parameter k_2 and the thickness d_2 of the upper layer. The fulcrum point shown is common to both layers. Based on the fact that the contraction force in the upper layer is relatively large and that the lower Au–plastic layer isn't contractible (F_1^i at the interface is 0), we assume that the stress at the fulcrum at the interface is only from the contraction of the upper layer. Then the stress on this point is equal to the remaining contracting force at the bottom of the upper layer and we note it as F_2^0. And the remaining contracting force on the top of the upper layer can be expressed as $(F_2^0 - k_2\theta d_2)$. Based on assumption (1), the average stress along the upper layer after bending is complete can be expressed as:

$$F_2^{\text{average}} = \frac{(F_2^0 - k_2\theta d_2) + F_2^0}{2} \quad (1)$$

Likewise, the forces on the plastic–Au layer increase as the distance from the interface increases. Again, this can be related to a spring; at the interface where bending is most complete there is little restoring force, while there is still significant forces at the bottom where bending is less complete. These forces are noted as F_1^i (red vectors), which are in the same direction of the remaining contraction forces in the upper layer, which oppose bending due to the fulcrum. The bending angle θ together with material related force parameter k_1 and thickness d_1 of the lower layer determines the restoring forces along the lower layer. As shown in Figure 2b, the stress at the bottom of the lower layer was noted as F_1^0, which can be expressed as $(k_1\theta d_1)$. Because the Au–plastic layer is not contractible, the stress on the fulcrum from the bottom layer is 0. Thus, the average stress in this layer can be expressed as:

$$F_1^{\text{average}} = \frac{k_1\theta d_1 + 0}{2} \quad (2)$$

Due to stresses on both layers two torques are formed on both layers separately, which are expressed mathematically below:

$$\tau_1 = F_1^{\text{average}} \times \gamma_1 = \frac{k_1\theta d_1 + 0}{2} \times \frac{d_1}{2} \quad (3)$$

$$\tau_2 = F_2^{\text{average}} \times \gamma_2 = \frac{F_2^0 - k_2\theta d_2 + F_2^0}{2} \times \frac{d_2}{2} \quad (4)$$

represents the distance from the point where the torque is measured to the point where the force is applied in the respective layers, while d is the thickness of the respective layers. In each Equation, γ is equal to half of the thickness of each layer. At the final state of bending ("equilibrium"), the two torques are equal to maintain a steady bent state, otherwise, the assembly will continue to bend until this is the case. As such, after complete bending Equations 3,4 are equal leading to:

$$\frac{k_1\theta d_1 + 0}{2} \times \frac{d1}{2} = \frac{F_2^0 - k_2\theta d_2 + F_2^0}{2} \times \frac{d_2}{2} \quad (5)$$

Then the microscopic bending angle θ can be expressed as:

$$\theta = \frac{2d_2F_2^0}{k_1d_1^2 + k_2d_2^2} \quad (6)$$

Again, this is the "microscopic" bending angle, which leads to macroscopic device bending. Macroscopically the device will show specific curvature after bending is complete. Theoretically, we can represent the curvature by the radius (R) of rolls or incomplete rolls after bending. In this case, microscopically $F_2{}^0$ in Equation 6 can be expressed as one force (between the upper layer and the lower layer), which is determined by another force parameter, the interfacial force parameter (k) multiplied by a length (L), which represents the length of the interfacial layer exerting forces on the fulcrum on the microscopic level. Furthermore, L can be expressed as the bending angle θ multiplied by $(R - d_1)$. Therefore, $F_2{}^0$ can be represented by:

$$F_2^0 = k\theta(R - d_1) \quad (7)$$

Subsequently, Equation 6 can be rewritten as:

$$\theta = \frac{2d_2k\theta(R - d_1)}{k_1d_1^2 + k_2d_2^2} \quad (8)$$

Finally, the macroscopically observed R can be expressed as:

$$R = \frac{k_1d_1^2/k + k_2d_2^2/k}{2d_2} + d_1 \quad (9)$$

As k, k_1, k_2 are force parameters (constants) determined by the materials themselves, from Equation 9 we conclude that the radius after bending is only related to the thickness of each layer d_1 and d_2.

To test our mathematical model, we fabricated rectangular devices of different dimension, but containing the same upper and lower layer thicknesses. As predicted from Equation 9, these devices should self-fold to yield similar values for R. There is a precedent for this result; in a previous study, Li and co-workers[26] observed that the curvature of rolls after bending of rectangular bilayers depended on the thickness of the layers and strain, but not the bilayer dimensions. While this is the case, our investigation is the first to develop and test a mathematical model that is capable of predicting the self-folding behavior of such materials. Furthermore, we investigated how the bending of a single device, with given dimensions, depended on the upper layer thickness (d_2) to determine if Equation (9) could indeed be used to predict R.

2.2. Results

2.2.1 Self-Folding Behavior of Rectangular Devices

Self-folding is a term used to describe materials that transform autonomously from two-dimensional materials into three dimensional structures such as spirals, tubes, corrugated sheets or polyhedron.[27] Self-folding can take place on many length scales—from meters to nanometers.[28,29] Here, we show that the self-folding behavior of materials with centimeter-scale dimensions can be predicted using Equation 9. To accomplish this, we fabricated rectangular devices (see Figures 1, 2) with four different aspect ratios. Furthermore, for each aspect ratio, we fabricated devices of different overall dimensions. In each case, the amount of pDADMAC added to each device was scaled for their individual dimensions such that the amount of pDADMAC on a given device area was the same from device to device. Therefore, the thickness of the upper layer (d_2) was constant. Furthermore, the devices were constructed from the same lower layer material, maintaining the same lower layer thickness (d_1) from device to device. **Figure 3**a is a photograph of a representative device (3 cm × 9 cm) with pDADMAC deposited in its unfolded state (high humidity), while Figure 3b shows the final state of the devices dried under the same conditions. It is interesting to note that the devices tend to self-fold into unique three-dimensional structures after drying, which will be the subject of a future investigation. Here, we were interested in the radius of curvature (R in Equation 9 and how that depended on the device's aspect ratio and size. To measure the radius of curvature, we used the approach shown schematically in Figure 4. The circle in **Figure 4** represents a device in its final state. If two lines are drawn (AB and $A'B$), perpendicular to the radii (OA and OA') they intersect at point B. As a result, two triangles are formed. In δOAB, the length AB can be measured using two rulers placed on the tangents to the curvature of the device—the "length" at the intersection point is AB. Furthermore, the angle between the two rulers at that condition is also measured. With this information, the radius OA could be determined using:

$$\tan\frac{\alpha}{2} = \frac{OA}{AB} \quad (10)$$

$$OA = AB \times \tan\frac{\alpha}{2} \quad (11)$$

For each device, we measured the radius at 5 different locations at a humidity of 19.7% and temperature of 23 °C and plotted the average radius as a function of the area (length ×

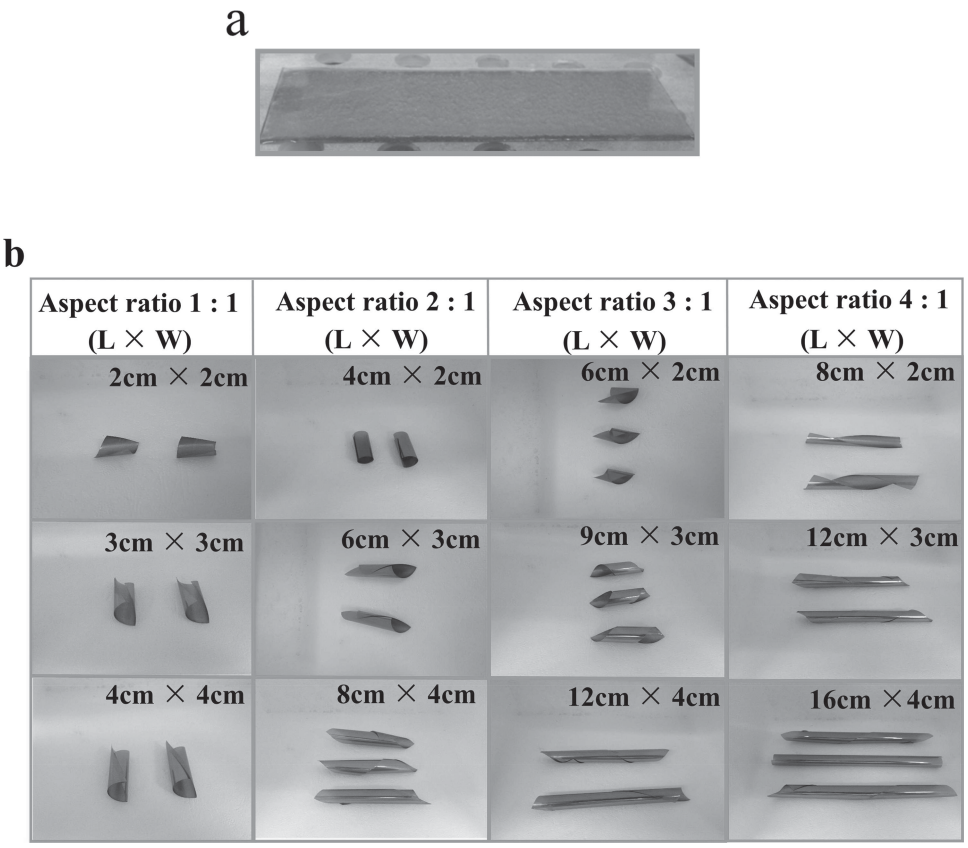

Figure 3. Images of devices before and after bending. a) A photograph of a device with dimensions of 3 cm × 9 cm before bending. b) Devices of different aspect ratio and dimensions after bending. As can be seen, the devices form different 3D structures after bending dependent on the aspect ratio and size of the devices. *L* represents the length of the device, while *W* is the width.

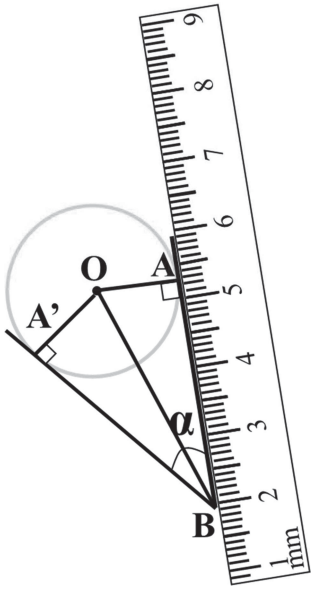

Figure 4. Protocol used for measuring the radius of the devices after bending. *AB* and *A′B* are two tangents perpendicular to the radius of a device *OA* and *OA′*, respectively. *B* is the intersection of the two tangents. α is the angle between the two tangents. Two rulers were used to measure *AB* and *A′B*, while a protractor was used to measure the angle between the rulers to determine α.

width) for each aspect ratio. The data is shown in **Figure 5**. As can be seen, while the individual devices may self-fold into different structures (tubes/spirals), the radius of curvature for all the devices, regardless of overall size or aspect ratio, is in the range of 0.75–0.85 cm. From these results, we conclude that the final radius of the devices only depends on the thickness of the two layers. Again, investigations into the self-folding into different structures will be the subject of a future publication.

In addition, using devices with dimensions of 9 cm × 3 cm, the thickness of the upper layer d_2 was systematically varied by depositing different amounts of pDADMAC solution on the surface of the microgel–Au–plastic substrate. In this case, the thickness of Au–plastic substrate was kept constant. The volumes of pDADMAC used were 1–10 mL, which yielded a range of d_2 (see Supporting Information), and two devices of each thickness were prepared for each volume. Following drying of the pDADMAC layer, its thickness was measured using a digital caliper and the radius of curvature was measured for each device using the same protocol as above. The data is plotted in **Figure 6**. As can be seen, the radius of curvature depends dramatically on the thickness of the upper layer. Subsequently, by knowing the thicknesses of both layers, we could fit Equation 12 to the data in Figure 6, and the best fit values for *A* and *B* determined. It should be pointed out here that Equation 12 is the same as Equation 9 with the constants *A* and *B* representing the individual *k*-containing terms in Equation 9. As a result of

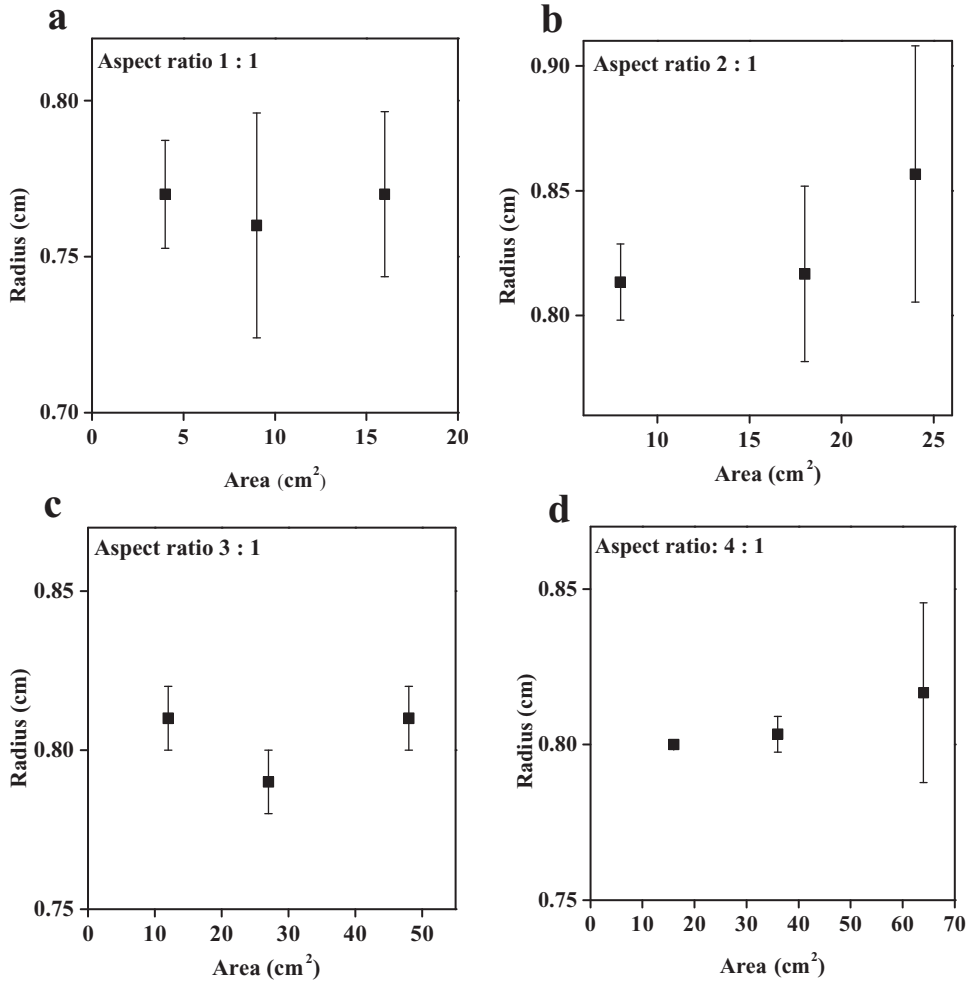

Figure 5. The measured radius of the devices as a function of their size and aspect ratio. As can be seen, the measured radius of the devices didn't depend strongly on their size and aspect ratio. Three devices were made at each size and aspect ratio and the radius determined at 5 different locations for each device. Each point is therefore the average of 15 radius values measured from 3 devices at 5 different locations. The error bars indicate the standard deviation.

the fit, the best fit values for A and B in Equation 12 were found to be 3.6 ± 0.4 and 15.1 ± 2.4, respectively.

$$R = \frac{A + Bd_2^2}{2d_2} + 0.1016 \tag{12}$$

Further, we tested the model by fabricating device with given d_2 and comparing the predicted and measured R values. For d_2 of 0.45 mm, and 0.72 mm, the model predicts an R of 7.40 mm and 8.02 mm. This is in comparison to the measured values of 6.63 mm and 8.43 mm, as can be seen the model closely predicts the experimental R.

2.2.2. Controlling the Self-Folding Process

Using our mechanical and mathematical models above to predict important design parameters, we created materials that are capable of self-folding into desired 3D structures. To accomplish this, an empirical rule was developed to calculate the amount of pDADMAC–microgel composite needed to be added to the Au–plastic substrate to make the whole device self-fold by a specific angle α. Equation 13 was developed to predict this behavior:

$$\widehat{AA'}; = \frac{180^\circ - \alpha}{360^\circ} \times 2\pi \times OA \tag{13}$$

Wherein, is the length of the arc AA' in Figure 4, while OA is the radius of the self-folded structure at a specific humidity and temperature. $2\pi \times OA$ is the circumference of the self-folded device. For example, at humidity of 19.7% (dry) and temperature of 23 °C, if we want a structure with a curling angle α of 90°, we need the length of to be ≈1.25 cm according to the Equation 13. That means, if we want the device to bend to yield a right angle, we need to deposit a layer of pDADMAC onto the device with a width of ≈1.25 cm along the direction of bending. The volume of pDADMAC added to the device should yield the same d_2 as used above. Following this rule, we designed devices capable of self-folding into discrete and predetermined 3D

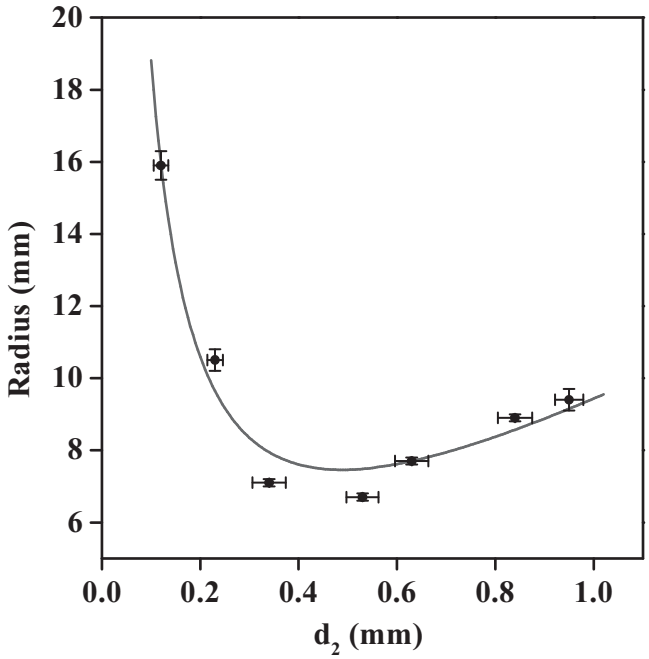

Figure 6. Dependence of device radius on pDADMAC layer thickness. The data points are real data obtained by measuring the radius of two separate devices with a given d_2. Each point is the average of 10 radii determined at 5 different locations of the two separate devices. The error bars are the standard deviations of the measured d_2 and radius. The solid line is the best fit of Equation 12 to the data yielding values for A and B of 3.6 ± 0.4 and 15.1 ± 2.4, respectively. The Equation was fit to the data using MATLAB software.

structures. As can be seen in **Figure 7**, the width and direction of the deposited pDADMAC layer depends on how we want the device to self-fold, and through this, we have great control over the device's self-folding behavior.

3. Conclusion

In summary, we investigated in detail the self-folding behavior of rectangular humidity-responsive microgel-based polymer composites deposited on a substrate of varying dimensions and aspect ratios. We detailed a mechanical and mathematical model that is capable of describing the self-folding characteristics of these bilayer devices. Furthermore, using this information, we were able to devise an approach for fabricating devices that self-fold into predetermined 3D structures with varying complexities. We hypothesize that the material parameters defined in the presented model is one that can be generalized to essentially any bilayer material, and similar studies can be completed. This work paves the way for producing stimuli responsive adaptive polymer materials, which have potential applications in actuation, sensing, artificial muscles and robotics.

4. Experimental Section

Materials: *N*-isopropylacrylamide was purchased from TCI (Portland, Oregon) and purified by recrystallization from hexanes (ACS reagent grade, EMD, Gibbstown, NJ) prior to use. N, N-methylenebisacrylamide (BIS) (99%), acrylic acid (AAc) (99%), and ammonium persulfate (APS) (98+%) were obtained from Sigma-Aldrich (Oakville, Ontario) and were used as received. Poly (diallyldimethylammonium chloride) solution, pDADMAC of MW <100 000 (20% in water) were purchased from Sigma-Aldrich (St. Louis, MO). Deionized (DI) water with a resistivity of 18.2 MΩ cm was used. Cr/Au annealing was done in a Thermolyne muffle furnace from Thermo Fisher Scientific (Ottawa, Ontario). Anhydrous ethanol was obtained from Commercial Alcohols (Brampton, Ontario). Fisher's finest glass coverslips were 25 mm × 25 mm and obtained from Fisher Scientific (Ottawa, Ontario). Cr was 99.999% and obtained from ESPI (Ashland, OR), while Au was 99.99% and obtained from MRCS Canada (Edmonton, AB).

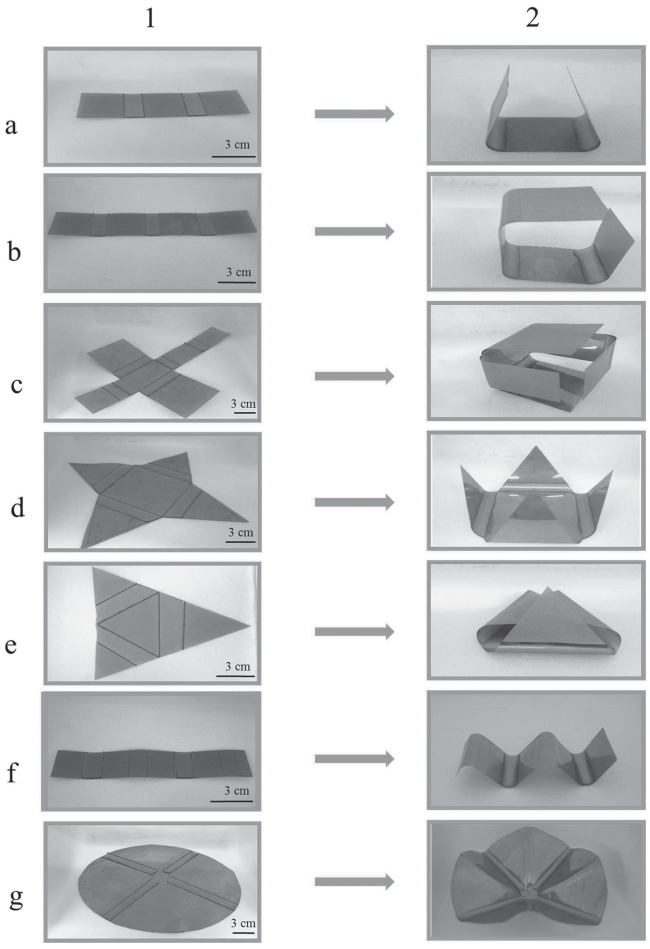

Figure 7. Rationally designed devices capable of self-folding into three-dimensional structures. Column 1) Specially designed microgel coated Au–plastic substrates with a given width of pDADMAC deposited at specific locations (outlined areas) to yield the desired 3D structure Column 2) after drying. For devices (a–d), the width of the pDADMAC solution deposited in each frame was around ≈1.25 cm. For device (e), the width of the pDADMAC solution was ≈2 cm. For devices f and g both sides of the plastic substrates were coated with Au and microgels, and pDADMAC subsequently deposited on specific locations with a width of ≈1.25 cm.

Microgel Synthesis: Microgels composed of poly(*N*-isopropylacrylamide)-co-acrylic acid (pNIPAm-co-AAc) were synthesized via radical precipitation polymerization as described previously.[21] The monomer mixture, with a total concentration of 154 mM, was comprised of 85% (mole/mole) NIPAm, 10% AAc, and 5% BIS as the crosslinker. NIPAm (17.0 mmol), and BIS (1.0 mmol) were dissolved in deionized water (100 mL) with stirring in a beaker. The mixture was filtered

through a 0.2 μm filter affixed to a 20 mL syringe into a 200 mL 3-neck round-bottom flask. The beaker was rinsed with 25 mL of deionized water and then filtered into the NIPAm/BIS solution. The flask was then equipped with a temperature probe, a condenser and a N_2 gas inlet. The solution was bubbled with N_2 gas for ≈1.5 h, while stirring at a rate of 450 rpm, allowing the temperature to reach 45 °C. AAc (2.0 mmol) was then added to the heated mixture with a micropipette in one aliquot. A 0.078 M aqueous solution of APS (5 mL) was delivered to the reaction flask with a transfer pipet to initiate the reaction. Immediately following initiation, a temperature ramp of 45 to 65 °C was applied to the solution at a rate of 30 °C h^{-1}. The reaction was allowed to proceed overnight at 65 °C. After polymerization, the reaction mixture was allowed to cool down to room temperature and filtered through glass wool to remove any large aggregates. The coagulum was rinsed with deionized water and filtered. Aliquots of these microgels (12 mL) were centrifuged at a speed of ≈8500 relative centrifugal force (rcf) at 23 °C for ≈40 min to produce a pellet at the bottom of the centrifuge tube. The supernatant was removed from the pellet of microgels, which was then re-suspended to the original volume (12 mL) using deionized water. This process was repeated until the microgels were cleaned.

Fabrication of Plastic Substrates: Transparent flexible plastic sheets (transparency films for high temperature laser copiers from 3M company, Canada) were rinsed with DI water and ethanol and dried with N_2 gas, and 2 nm of Cr followed by 50 nm of Au were thermally evaporated onto them at a rate of ≈0.2 Å s^{-1} and ≈0.1 Å s^{-1}, respectively, using a Torr International Inc. model THEUPG thermal evaporation system (New Windsor, NY). The Cr acts as adhesion layer to hold the Au layer on the plastic. An aliquot of about 12 mL of previously purified microgel solution was centrifuged for 30 min at 23 °C at ≈ 8500 relative centrifugal force (rcf) to pack the microgels into a pellet at the bottom of the tube. After removal of the supernatant solution, the microgel pellet was vortexed and placed onto a hot plate at 30 °C. A previously coated Cr/Au substrate was rinsed with ethanol, dried with N_2, and then placed onto hot plate (Corning, NY) set to 30 °C. Aliquots (40 μL for each 25 mm × 25 mm area) of the concentrated microgels were put onto the substrate and then spread toward each edges using the side of a micropipette tip, as previously described.[30] The microgel solution was allowed to dry completely on the substrate for 2 h with the hot plate temperature set to 35 °C. After 2 h, the dry film was rinsed copiously to remove any unreacted monomer and/or linear polymer from the microgel solution. Then the substrates were washed copiously with DI water to remove any excess microgels not bound directly to the Au. Microgel painted substrate was then placed into a DI water bath and allowed to incubate overnight on a hot plate set to ≈30 °C. Following this step, the substrate was again rinsed with DI water to further remove any microgels not bound directly to the Au substrate surface. The microgel painted Au coated substrate was dried with N_2 gas and used for the experiment.

Self-Folding Devices: A specific amount of pDADMAC solution (pH 6.5, 20 wt% in water) was spread onto the microgel layer. The whole set up was undisturbed and dried at ambient temperature/humidity. After the complete drying of the film, the devices were moved into the chamber, which can control the environmental humidity. Air-O-Swiss AOS 7145 Cool Mist Ultrasonic humidifier (manufactured by Swiss Pure Air) was used to control the humidity in the chamber with an electronic feedback mechanism to maintain a steady humidity.

Supporting Information

Supporting Information is available from the Wiley Online Library or from the author.

Acknowledgments

M.J.S. acknowledges funding from the University of Alberta (the Department of Chemistry and the Faculty of Science), the Natural Science and Engineering Research Council (NSERC), the Canada Foundation for Innovation (CFI), the Alberta Advanced Education & Technology Small Equipment Grants Program (AET/SEGP) and Grand Challenges Canada. M.J.S. acknowledges Mark McDermott for the use of the thermal evaporator.

Received: January 20, 2014
Published online: April 1, 2014

[1] G. Stoychev, S. Turcaud, J. W. C. Dunlop, L. Ionov, *Adv. Funct. Mater.* **2013**, *23*, 2295–2300.
[2] R. Fuhrer, E. K. Athanassiou, N. A. Luechinger, W. J. Stark, *Small* **2009**, *5*, 383–388.
[3] K. Liu, C. Cheng, Z. Cheng, K. Wang, R. Ramesh, J. Wu, *Nano Lett.* **2012**, *12*, 6302–6308.
[4] S. Alben, B. Balakrisnan, E. Smela, *Nano Lett.* **2011**, *11*, 2280–2285.
[5] M. R. Islam, X. Li, K. Smyth, M. J. Serpe, *Angew. Chem. Int. Ed.* **2013**, *52*, 10330–10333.
[6] C. M. Yakacki, N. S. Satarkar, K. Gall, R. Likos, J. Z. Hilt, *J. Appl. Polym. Sci.* **2009**, *112*, 3166–3176.
[7] T. Fukushima, K. Asaka, A. Kosaka, T. Aida, *Angew. Chem. Int. Ed.* **2005**, *117*, 2462–2465.
[8] S. V. Ahir, Terentjev, E. M , *Nat. Mater.* **2005**, *4*, 491–495.
[9] R. Yoshida, K. Uchida, Y. Kaneko, K. Sakai, A. Kikuchi, Y. Sakurai, T. Okano, *Nature* **1995**, *374*, 240–242.
[10] J. Kopecek, *Nature* **2002**, *417*, 388–391.
[11] Z. Hu, X. Zhang, Y. Li, *Science* **1995**, *269*, 525–527.
[12] J. Kim, J. A. Hanna, M. Byun, C. D. Santangelo, R. C. Hayward, *Science* **2012**, *335*, 1201–1205.
[13] H. Thérien-Aubin, Z. L. Wu, Z. Nie, E. Kumacheva, *J. Am. Chem. Soc.* **2013**, *135*, 4834–4839.
[14] E. Wang, M. S. Desai, S.-W. Lee, *Nano Lett.* **2013**, *13*, 2826–2830.
[15] J. R. Kumpfer, S. J. Rowan, *J. Am. Chem. Soc.* **2011**, *133*, 12866–12874.
[16] M. Ma, L. Guo, D. G. Anderson, R. Langer, *Science* **2013**, *339*, 186–189.
[17] Y. Ma, Y. Zhang, B. Wu, W. Sun, Z. Li, J. Sun, *Angew. Chem. Int. Ed.* **2011**, *50*, 6254–6257.
[18] C. Wu, S. Zhou, *Macromolecules* **1995**, *28*, 8381–8387.
[19] H. Kawaguchi, K. Fujimoto, Y. Mizuhara, *Colloid Polym. Sci.* **1992**, *270*, 53–57.
[20] M. J. Serpe, L. A. Lyon, *Chem. Mater.* **2004**, *16*, 4373–4380.
[21] C. D. Sorrell, M. J. Serpe, *Adv. Mater.* **2011**, *23*, 4088–4092.
[22] M. J. Serpe, K. A. Yarmey, C. M. Nolan, L. A. Lyon, *Biomacromolecules* **2004**, *6*, 408–413.
[23] M. R. Islam, M. J. Serpe, *Macromolecules* **2013**, *46*, 1599–1606.
[24] J. A. Jaber, J. B. Schlenoff, *Macromolecules* **2005**, *38*, 1300–1306.
[25] N. A. Kotov, T. Haraszti, L. Turi, G. Zavala, R. E. Geer, I. Dekany, J. H. Fendler, *J. Am. Chem. Soc.* **1997**, *119*, 6821–6832.
[26] I. S. Chun, A. Challa, B. Derickson, K. J. Hsia, X. L. Li, *Nano Lett.* **2010**, *10*, 3927–3932.
[27] T. G. Leong, A. M. Zarafshar, D. H. Gracias, *Small* **2010**, *6*, 792–806.
[28] J.-H. Cho, A. Azam, D. H. Gracias, *Langmuir* **2010**, *26*, 16534–16539.
[29] J.-H. Cho, M. D. Keung, N. Varellen, L. Lagae, V. V. Moshchalkov, P. V. Dorpe, D. H. Gracias, *Small* **2011**, *7*, 1943–1948.
[30] C. D. Sorrell, M. C. D. Carter, M. J. A. Serpe, *ACS Appl. Mater. Interfaces* **2011**, *3*, 1140–1147.